Direct Monte Carlo simulations of the equilibrium properties of *n*-pentane liquid–vapor interface

Florent Goujon and Patrice Malfreyt[a)]
Laboratoire de Thermodynamique des Solutions et des Polymères, UMR 6003 CNRS, Université Blaise Pascal, 63177 Aubière Cedex, France

Anne Boutin and Alain H. Fuchs
Laboratoire de Chimie Physique, UMR 8000 CNRS, Université Paris-Sud, 91405 Orsay, France

(Received 24 December 2001; accepted 18 February 2002)

Direct MC calculations have been carried out to study the liquid–vapor equilibrium of *n*-pentane. We have used the local long range correction to the configurational energy within the Metropolis scheme and an algorithm allowing us to select randomly with equal probability two different maximum displacements. The thermal equilibrium conditions are checked by calculating the profiles of the configurational temperature in the vapor and liquid phases. We also check the mechanical equilibrium by calculating the profiles of the normal and tangential pressure components. The normal pressure profile is constant through the interface and in both phases on the conditions that the two parts of the long range corrections to the normal pressure area included in the calculations. The critical densities and temperatures are well predicted and the vapor pressures agree satisfactory with the experimental values within larger statistical fluctuations. The long range corrections to the surface tension are calculated using various analytical forms and are included in the computation to give values which are in good agreement with those available in the literature. Finally, the surface tension is computed from 299 K to 425 K for two system sizes and three cutoff values. © *2002 American Institute of Physics.* [DOI: 10.1063/1.1468216]

I. INTRODUCTION

A knowledge of the phase behavior of hydrocarbons is of great importance in many technological applications in the petrochemical industry. Although the liquid–vapor phase equilibria of hydrocarbons have been studied extensively during the last decade, the development of new algorithms and potential models still represents an area of active research.

Among these algorithms, the Gibbs Ensemble Monte Carlo method (GEMC) (Refs. 1–3) has been applied successfully to calculate the vapor–liquid and liquid–liquid coexistence curves of hydrocarbon systems. This technique has been improved by the use of the configurational statistical bias method of Smit *et al.*[4] to perform the insertion of hydrocarbon chains in the dense phase atom by atom. An additional bias for the insertion of the first bead of the alkane chain has also been applied.[5,6]

Many different models [OPLS (Ref. 7), SKS (Ref. 8), TraPPE (Ref. 9)] based on the United-Atom description have been developed. It has been shown that the TraPPE force field is the most appropriate model using the UA description of reproducing accurately the vapor–liquid coexistence densities and critical properties of linear alkanes from methane to dodecane.[9] Toxvaerd has proposed an Anisotropic United Atom Potential which performs better for predicting equations of state of alkanes at high pressure.[10–12] New parameters of the Anisotropic United Atom Potential (AUA4 version)[13] have been proposed and have yielded better predictions of the critical points and of the equilibrium properties of pure *n*-alkanes in a large range of temperatures and hydrocarbon chain lengths.

Whereas GEMC simulations are performed in two separate boxes, the direct method using MD or MC algorithms consists of simulating the two phase regions physically in contact with the presence of an explicit interface. The increase of computing power makes this method more and more attractive and straightforward for studying phase equilibria of alkanes. This technique yields microscopic information on the interface region and thermodynamic quantities such as surface tension. It has been extensively applied to LJ fluids[14–16] but not widely applied to hydrocarbons systems.[17,18] Simulations with an explicit interface highlight the difficulty of estimating the long range corrections due to the nonuniformity of the density distribution. Some authors have used a truncated and shifted potential in the MD simulations in order to deal with a continuous force function.[19] A recent study on LJ fluid[20] underlines that in MC calculations, most of the simulations use the truncated potential, whereas in MD simulations the forces usually correspond to the truncated and shifted potential. As a consequence, MC calculations with truncated potential should be compared to MD simulations with truncated forces plus an additional term due to the discontinuity of the truncated potential at the cutoff distance.[20] The comparison between MC and MD results is not so straightforward and has to be done carefully particularly in the case of two phase systems where the truncation of the interactions can be of great importance as far as equi-

a)Author to whom correspondence should be addressed. Electronic mail: patrice.malfreyt@univ-bpclermont.fr

 © 2002 American Institute of Physics

This article is copyrighted as indicated in the article. Reuse of AIP content is subject to the terms at: http://scitation.aip.org/termsconditions. Downloaded to IP: 128.178.157.170 On: Mon, 15 Sep 2014 09:19:59

librium properties of the system are concerned. In addition, this work[20] also establishes that the normal pressures are constant in the vapor and liquid phase in Lennard-Jones fluid using both MC and MD techniques.

In this paper, we focus on the thermal and mechanical equilibrium of the liquid–vapor interface of *n*-pentane. However, our approach differs from the work of Alejandre *et al.*[20] and consists of using the long range corrections developed by Guo and Lu[21] and in incorporating these to the configurational energy within the simulations. In a previous paper,[22] we have validated our Monte Carlo algorithm by checking the coexisting densities and critical points for the *n*-pentane and *n*-decane molecules. We have used the local range correction energy in conjunction with an algorithm allowing to select randomly with equal probability two different displacements. The present study also aims at investigating the system size dependence of the thermodynamic properties (vapor pressure, temperature, surface tension, critical points) for the *n*-pentane molecule. An effort is made to check by using the long range corrections developed by Guo and Lu[21] that the normal and tangential pressure components as well as the temperature profiles are consistent throughout the vapor and liquid phases for a molecular system for which not many studies have been carried out. We test different expressions for the long range corrections to the surface tension to emphasize the role of the system size for these tail corrections. To allow a better comparison for the set of simulations already performed, we decide to use in our simulations the TraPPE force field.

The paper is arranged as follows: In Sec. II, we present a description of the intramolecular and intermolecular functions of the TraPPE force field. Section III contains the computational procedures we have employed in our simulations. In Sec. IV, we present the operational expressions for the configurational temperature, the components of the pressure tensor calculated using two different definitions and for the surface tension with the corresponding long range corrections. Section V presents the results of these simulations and relates these to experimental data. Finally, in Sec. VI, we draw the main conclusions from our work.

II. THE POTENTIAL MODEL

The *n*-pentane molecule is modeled as a flexible molecule containing five united atoms with interaction sites located at each carbon atom. In this study, we use the parameters of the TraPPE force field.[9] In this model, the nonbonded interactions between pseudo-atoms which are separated by more than three chemical bonds or belong to different molecules are calculated using the Lennard-Jones potential,

$$u_{\mathrm{LJ}}(r_{ij}) = 4\epsilon_{ij}\left[\left(\frac{\sigma_{ij}}{r_{ij}}\right)^{12} - \left(\frac{\sigma_{ij}}{r_{ij}}\right)^{6}\right], \tag{1}$$

where ϵ_{ij} is the energy parameter of the interaction, σ_{ij} is the Lennard-Jones core diameter, and r_{ij} is the distance between interaction sites i and j. The LJ parameters for the interactions between unlike atoms are calculated by using the Lorentz–Berthelot mixing rules,

TABLE I. Number of *n*-pentane molecules, box dimensions, cutoff value, and the range of Boltzmann temperatures simulated. The total CPU time for the MC simulations over 80 000 cycles is compared with the CPU time for the calculation of the long range correction to the pressure components over 10 000 configurations with a 1 GHz PC.

N	Lx/Å	Ly/Å	Lz/Å	r_c/Å	T/K	t (MC)/h	t (lrc)/h
400	35	35	200	13.0	[299;425]	123	14
400	35	35	200	15.0	[299;425]	136	14
400	35	35	200	17.0	[299;425]	144	14
600	35	35	250	13.0	[299;425]	230	21
600	44	44	200	22.0	299	365	22

$$\epsilon_{ij} = (\epsilon_{ii}\epsilon_{jj})^{1/2}, \quad \sigma_{ij} = \tfrac{1}{2}(\sigma_{ii} + \sigma_{jj}). \tag{2}$$

The interaction sites have the following Lennard-Jones parameters: $\epsilon_{\mathrm{CH_3}}/k_B = 98$ K and $\epsilon_{\mathrm{CH_2}}/k_B = 46$ K, where k_B is Boltzmann's constant. The size parameters are $\sigma_{\mathrm{CH_3}} = 3.75$ Å and $\sigma_{\mathrm{CH_2}} = 3.95$ Å.

In the TraPPE model, the intramolecular interactions include contributions from bond angle bending interactions, torsional interactions, and nonbonded interactions. The bond lengths are fixed to 1.54 Å. The bond angle potential has the following form:

$$u_{\mathrm{bend}} = \tfrac{1}{2}k_\theta(\theta - \theta_0)^2, \tag{3}$$

where θ is the angle between three consecutive united atoms, $k_\theta/k_B = 62\,500$ K rad^{-2} is the bending angle, $\theta_0 = 114°$ is the equilibrium bond angle.

For the torsional function, we used the Jorgensen potential,[7]

$$u_{\mathrm{tors}} = 0.5c_1(1+\cos\phi) + 0.5c_2(1-\cos 2\phi) + 0.5c_3(1+\cos 3\phi), \tag{4}$$

where ϕ is the dihedral angle between four subsequent united atoms, $c_1/k_B = 355.03$ K, $c_2/k_B = 68.19$ K, $c_3/k_B = 791.32$ K.

As mentioned above, the intramolecular nonbonded interactions are represented by the Lennard-Jones function with the same potential parameters as used for the corresponding intermolecular potentials.

III. COMPUTATIONAL TECHNIQUES

The simulations have been carried out in the NVT ensemble in a rectangular parallelepiped box of dimensions $L_xL_yL_z$ ($L_x = L_y$) with periodic conditions in all the directions. Intermolecular interactions have been computed to a certain cutoff r_c. The details of the simulations are summarized in Table I. The simulations have been performed in cycles. Each cycle consists of N randomly selected Monte Carlo moves with fixed probabilities, N being equal to the total number of molecules. The Monte Carlo moves we perform are (1) translation of the center-of-mass of a random molecule, (2) rotation of a randomly selected molecule around its center-of-mass, (3) regrowing of part of random molecule using the configurational-bias scheme. The relatives probabilities with which trial moves are attempted are set to 45% for the displacement, 35% for the rotation, and

This article is copyrighted as indicated in the article. Reuse of AIP content is subject to the terms at: http://scitation.aip.org/termsconditions. Downloaded to IP: 128.178.157.170 On: Mon, 15 Sep 2014 09:19:59

20% for the change of the internal configuration of a molecule. Thus, the maximum displacement and maximum rotation are adjusted during the equilibrium phase to give an acceptance ratio of 0.4. For the modification of the conformation of a molecule, we use the configurational bias Monte Carlo technique and we select randomly a molecule and the number of atoms to be regrown. The number of trial orientations is equal to 5. Using this procedure, we have obtained an acceptance probability for the modification of the internal structure which range from 37% at $T=299$ K to 56% at $T=425$ K for pentane. As concerned the translational moves, we have also tested an algorithm allowing to use randomly with equal probability two different maximum displacements. The two maximum displacements are adjusted separately during the equilibration phase to give acceptance ratios of 20% and 60%, respectively. The final acceptance ratio for the translational move is kept to 40%. The first maximum displacement selected with a probability 0.2 increases from 0.9 Å ($T=299$ K) to 2.5 Å ($T=425$ K), whereas the second maximum displacement chosen with a probability 0.6 increases from 0.30 Å to 0.55 Å. This procedure improves the sampling of the configuration space of the vapor phase by allowing larger displacements. A Verlet neighbor list is implemented in the code using a list sphere radius r_l depending on the type of moves. The difference value $(r_l - r_c)$ is equal to 2.0 Å for the translational move, to 5.5 Å for the rotational move, and 10.5 Å for the internal configurational change.

In this work, we have calculated the long range corrections to the configurational energy in the z direction perpendicular to the interface. The cell is divided into slabs of width δz. The long range corrections to the total energy within each kth slab are defined by two parts,

$$\begin{aligned} u_{\mathrm{lrc}}(z_k) &= u_{\mathrm{lrc}}^{(1)}(z_k) + u_{\mathrm{lrc}}^{(2)}(z_k) \\ &= \frac{8\pi}{3}\rho(z_k)^2 V_s \sum_a^5 \sum_b^5 \epsilon_{ab}\left[\frac{1}{3}\left(\frac{\sigma_{ab}^{12}}{r_c^9}\right) - \left(\frac{\sigma_{ab}^{6}}{r_c^3}\right)\right] \\ &\quad + \pi\rho(z_k) V_s \int_{r_c}^{\infty} dr \int_{-r}^{r} d\Delta z \\ &\quad \times \sum_{i=1}^{n_z} [\rho(z_i) - \rho(z_{i-1})] r U_{\mathrm{L},m}(r), \end{aligned} \tag{5}$$

where $\rho(z_k)$ and V_s are, respectively, the density and the volume of the slab k. Δz is defined as the difference $z - z_k$. n_z is the number of slabs between z and z_k. $U_{\mathrm{LJ},m}(r)$ is the intermolecular energy between two pentane molecules and r is the distance between the two centers-of-mass,

$$U_{\mathrm{LJ},m}(r) = \sum_a^5 \sum_b^5 4\epsilon_{ab}\left[\left(\frac{\sigma_{ab}}{r}\right)^{12} - \left(\frac{\sigma_{ab}}{r}\right)^{6}\right]. \tag{6}$$

In the scheme proposed by Guo and Lu[21] for the implementation of the long range correction, we note that the tail corrections for the total configurational energy, the normal and tangential pressures can be divided into two parts. The first part of the long range contribution has an analytical form identical as that in the case of uniform density but uses the local density $\rho(z_k)$ of the slab. The second part consists of a double integral which contains a series of density differences which render this part cumbersome to calculate. As concerns the second part of the long range corrections to the total configurational energy, it has been shown[21] that it represents only a minor contribution of the total long range energy. We have also calculated this second term and evaluated the approximation made when we do not take into account this contribution. As a consequence, only the first part of the long range correction energy is included here in the total configurational energy. The total long range correction energy U_{lrc} is calculated by summing up all of the local contributions of each slab and is calculated after each move of molecular position. The U_{lrc} term is then added in the total energy of the system to be used in the Metroplis scheme.

The initial configuration has been generated by placing N pentane chains in a cubic box with random positions and by avoiding direct overlap with the molecules. An NpT Monte Carlo simulation has been performed over 20 000 cycles on this bulk fluid configuration. The resulting box has been surrounded by two empty cells in the z direction. A typical run for a given temperature consisted of 30 000 cycles (1.8×10^7 moves) for equilibration followed by a production phase of additional 50 000 cycles (3.0×10^7 moves) where thermodynamic and structural quantities were collected. The configurational temperature, the normal and tangential components of the pressure tensor as well as the surface tensions are calculated every 5 cycles during the production phase. The fluctuations in these values are estimated using the variations in 5 block averages of 2000 configurations. The equilibrated configuration was then used as the starting configuration for the next higher temperature. This procedure was repeated up to the highest temperature.

IV. THERMODYNAMIC PROPERITES

A. Configurational temperature

The configurational temperature[23–26] T_{conf} is calculated as a check from our Monte Carlo simulations from the following equation:

$$k_B T_{\mathrm{conf}} = \frac{|\nabla_r U|^2}{\nabla_r^2 U}, \tag{7}$$

where U is the intermolecular energy of the system and ∇_r represents the gradient operator with respect to the molecular position $\mathbf{r}$. After further elaboration, Eq. (7) leads to the following operational expression:

$$k_B T_{\mathrm{conf}} = \frac{\left\langle \sum_{i=1}^{N} F_i^2 \right\rangle}{\left\langle \sum_{i=1}^{N} \left(\frac{\delta F_{ix}}{\delta r_{ix}} + \frac{\delta F_{iy}}{\delta r_{iy}} + \frac{\delta F_{iz}}{\delta r_{iz}} \right) \right\rangle}, \tag{8}$$

where r_{ix}, r_{iy}, and r_{iz} refer to the Cartesian coordinates of $\mathbf{r_i}$. $\mathbf{F_i}$ is the intermolecular force on molecule i acting upon the molecular center-of-mass at $\mathbf{r_i}$ and is expressed as

$$\mathbf{F_i} = \sum_{j\neq i}^{N} \mathbf{F_{ij}} = \sum_{j\neq i}^{N} \sum_{a=1}^{5} \sum_{b=1}^{5} (f_{iajb}). \tag{9}$$

This article is copyrighted as indicated in the article. Reuse of AIP content is subject to the terms at: http://scitation.aip.org/termsconditions. Downloaded to IP: 128.178.157.170 On: Mon, 15 Sep 2014 09:19:59

This is equivalent to expressing $\mathbf{F_{ij}}$ as the sum of all the five site-site forces acting between pentane molecules. Using this definition, $\mathbf{F}_{ij}$ and $\mathbf{f}_{iajb}$, Eq. (10) is the intermolecular force between molecules *i* and *j* and the force between atom *a* in molecule *i* and atom *b* in molecule *j*, respectively. r_{iajb} denotes the distance between atom *a* in molecule *i* and atom *b* in molecule *j*,

$$\mathbf{f}_{iajb} = -\frac{\mathbf{r_{iajb}}}{r_{iajb}} \frac{dU_{\mathrm{LJ}}(r_{iajb})}{dr_{iajb}}. \tag{10}$$

The comparison between the configurational temperature and the Boltzmann temperature provides a check of our samplings in the canonical ensemble. The average slab temperature $T_{\mathrm{conf}}(z_k)$ in the slab *k* is defined as

$$k_B T_{\mathrm{conf}}(z_k) = \frac{\left\langle \sum_{i=1}^{N} H_k(z_i) F_i^2 \right\rangle}{\left\langle \sum_{i=1}^{N} H_k(z_i) \left(\frac{\delta F_{ix}}{\delta r_{ix}} + \frac{\delta F_{iy}}{\delta r_{iy}} + \frac{\delta F_{iz}}{\delta r_{iz}} \right) \right\rangle}, \tag{11}$$

where the slab width for sampling is $\delta z = 1.0$ Å. $H_k(z_i)$ is a tophat function with functional values of

$$\begin{cases} H_k(z_i) = 1 & \text{for } z_k - \dfrac{\delta z}{2} < z_i < z_k + \dfrac{\delta z}{2} \\ H_k(z_i) = 0 & \text{otherwise.} \end{cases} \tag{12}$$

z_i represents the *z*-position of the center of mass molecule *i*. The configurational temperature profile along the direction perpendicular to the interface has been calculated to ensure the constancy of the temperature in the vapor and liquid phases as required by the thermal equilibrium.

B. Pressure tensor components

The pressure tensor is composed of two parts, a kinetic part and a configurational part that arises from the intermolecular forces. The kinetic part is well defined whereas in an inhomogeneous system the second part may be defined in many ways. Two different forms have been developed to calculate the configurational part of the pressure tensor, one of the form described by Irving and Kirkwood[27] and one of the form described by Harasima.[28] The elements of the pressure tensor in the Irving–Kirkwood[29,30] definition (IK method) for a planar interface for a molecular system are given by the following expression:

$$p_{\alpha\beta}(z_k) = \langle \rho(z_k) \rangle k_B T \mathbf{I} + \frac{1}{A} \left\langle \sum_{i=1}^{N-1} \sum_{j>i}^{N} (\mathbf{r_{ij}})_\alpha (\mathbf{F_{ij}})_\beta \frac{1}{|z_{ij}|} \times \theta\left(\frac{z_k - z_i}{z_{ij}} \right) \theta\left(\frac{z_j - z_k}{z_{ij}} \right) \right\rangle. \tag{13}$$

In this equation, $\langle \cdots \rangle$ denotes an ensemble time average. $\rho(z_k)$ is the density profile along the *z* direction, $\mathbf{I}$ is the unit tensor, *T* is the absolute temperature, and k_B is Boltzmann's constant. α and β represent *x*, *y*, or *z* directions. $A = L_x \times L_y$ is the surface area. $\theta((z_k - z_i)/z_{ij})$ is the unit step function which is equal to 1 when $((z_k - z_i)/z_{ij}) > 0$ and zero otherwise. The distance z_{ij} between two molecular centers-of-mass is divided into slabs of width $\delta z = 1.0$ Å and the chains *i* and *j* contribute to the pressure tensor in a particular slab if the line joining *i* and *j*, crosses, starts or finishes in the slab. The contribution from the $i-j$ interaction is distributed uniformly along the line joining the centers-of-mass of chains *i* and *j*. The normal component $p_N(z_k)$ is equal to $p_{zz}(z_k)$ and the tangential component is defined according $p_T(z_k) = \frac{1}{2}(p_{xx}(z_k) + p_{yy}(z_k))$.

In this study, we use also an additional statistical mechanical technique based upon the method of planes[31,32] (MOP method) for calculating the configurational part of the pressure tensor. The $p_{\alpha z}$ component of the configurational part of the pressure tensor is given by

$$p_{\alpha z}(z_k) = \frac{1}{A} \sum_{i=1}^{N-1} \sum_{j>i}^{N} (\mathbf{F_{ij}})_\alpha [\theta(z_i - z_k)\theta(z_k - z_j) - \theta(z_j - z_k)\theta(z_k - z_i)]. \tag{14}$$

In the MOP method, the kinetic part is calculated from the momentum flux. Therefore, with MC calculations only the configurational part of the pressure may be calculated and compared with this calculated with the IK definition. If z_i and z_j are both either smaller or larger than z_k, the contribution to the pressure tensor is zero. If $z_i < z_k$ and $z_j > z_k$, then the first product of the Heaviside functions is zero while the second is unity. If $z_i > z_k$ and $z_j < z_k$, then the second is unity while the first is unity.

In the MOP method, the pressure is computed across each plane and z_k corresponds to the position of the plane *k* along the *z* direction. Consequently, only the p_{xz}, p_{yz}, and p_{zz} components may be calculated using the MOP formalism. Using the IK definition, z_k refers to the position of the *k*th volume element $(L_x \times L_y \times \delta z)$. The method of planes uses a well-defined mathematical procedure for the configurational part of the pressure tensor and it has been shown[31,32] that this technique is accurate. The comparison between the IK and MOP definitions will be made later throughout the paper.

The expressions of the long range corrections to the pressure in an inhomogeneous system with planar interfaces have been also developed by Guo and Lu[21] from this expressions of Irving and Kirkwood. The long range corrections to the normal pressure can be decomposed into two parts according Eq. (15),

$$\begin{aligned} p_{N,\mathrm{lrc}}(z_k) &= p^{(1)}_{N,\mathrm{lrc}}(z_k) + p^{(2)}_{N,\mathrm{lrc}}(z_k) \\ &= \frac{16\pi}{3} \rho^2(z_k) \sum_{a}^{5} \sum_{b}^{5} \epsilon_{ab} \left[\frac{2}{3} \left(\frac{\sigma_{ab}^{12}}{r_c^9} - \frac{\sigma_{ab}^{6}}{r_c^3} \right) \right] \\ &\quad - \pi \rho(z_k) \int_{r_c}^{\infty} dr \int_{-r}^{r} d\Delta z \sum_{i=1}^{n_z} [\rho(z_i) - \rho(z_{i-1})] \\ &\quad \times \frac{dU_{\mathrm{LJ},m}}{dr} (\Delta z)^2. \end{aligned} \tag{15}$$

As concerns the tangential pressure, only the second term is modified and is expressed by Eq. (16),

This article is copyrighted as indicated in the article. Reuse of AIP content is subject to the terms at: http://scitation.aip.org/termsconditions. Downloaded to IP: 128.178.157.170 On: Mon, 15 Sep 2014 09:19:59

$$p_{T,\mathrm{lrc}}^{(2)}(z_k) = -\frac{\pi}{2}\rho(z_k)\int_{r_c}^{\infty} dr \int_{-r}^{r} d\Delta z \times \sum_{i=1}^{n_s} [\rho(z_i)-\rho(z_{i-1})]\frac{dU_{\mathrm{LJ},m}}{dr}[r^2-(\Delta z)^2]. \tag{16}$$

These LRC contributions are added to the normal and tangential components of the pressure tensor calculated from the IK definition.

C. Surface tension

The surface tension can be therefore calculated by integrating the difference between the normal and tangential components of the pressure tensor across both interfaces,

$$\gamma_{\mathrm{IK}} = \frac{1}{2}\int_0^{L_z} [p_N(z)-p_T(z)]dz. \tag{17}$$

The factor $\frac{1}{2}$ is introduced to take into account the presence of two interfaces in the system. In this expression, the tail contributions for the normal and tangential pressure are not included. An alternative way to express the surface tension makes use of the molecular virial expression to give the following relationships:[33]

$$\gamma_m = \frac{1}{2A}\left\langle \sum_{i=1}^{N-1}\sum_{j=i+1}^{N}\sum_{a=1}^{5}\sum_{b=1}^{5} \frac{\mathbf{r_{ij}}\cdot\mathbf{r_{iajb}} - 3z_{ij}z_{iajb}}{2r_{iajb}} \times \frac{dU_{\mathrm{LJ}}(r_{iajb})}{dr_{iajb}} \right\rangle. \tag{18}$$

We have calculated the interfacial tension using both expressions Eq. (17) and Eq. (18) to check the consistency in the values resulted from our simulations. To calculate the long range corrections to the surface tension, we have used different expressions. For all these corrections, we assume that the radial pair distribution function $g(r_{ia},r_{ib})=1$. The first expression $\gamma_{(\mathrm{lrc},1)}$ (Refs. 34 and 35) based on the approximations that the interface thickness is zero and that the density of the vapor phase (ρ_v) is negligible, is expressed as

$$\gamma_{(\mathrm{lrc},1)} = \frac{3}{2}\pi\sum_{a=1}^{5}\sum_{b=1}^{5}\epsilon_{ab}\sigma_{ab}^6\left(\frac{\rho_l}{r_c}\right). \tag{19}$$

The second expression $\gamma_{(\mathrm{lrc},2)}$ (Ref. 18) considers that the density profile can be fitted to a hyperbolic tangent ant that for large separations, $r_{ij}=r_{iajb}$ and $z_{ij}=z_{iajb}$. We find thus

$$\gamma_{(\mathrm{lrc},2)} = \frac{\pi}{2}(\rho_l-\rho_v)^2\int_0^1 ds\int_{r_c}^{+\infty} dr\,\coth\left(\frac{2rs}{d}\right) \times \frac{dU_{\mathrm{LJ},m}}{dr} r^4(3s^3-s), \tag{20}$$

where d is an estimation of the thickness of the interface and s is a parameter defined as $z=(z_i-z_j)/r_{ij}$.

The following two expressions calculate the profiles along the z direction of the long range corrections to the surface tension. The expression in Eq. (21) (Refs. 36 and 37) divides the box in bins, each of which has a width δz and uses spherical coordinates r and θ,

$$\gamma_{(\mathrm{lrc},3)}(z_k) = \pi\int_{r_c}^{\infty} dr\int_0^{\pi} d\theta(1-3\cos^2\theta) \times \frac{dU_{\mathrm{LJ},m}}{dr}\rho(z_i+r\cos\theta)\sin\theta. \tag{21}$$

This expression does not require any analytical form of the density profile but uses the density profile of each configuration.

The last expression $\gamma_{(\mathrm{lrc},4)}$ was developed by Guo and Lu[21] and determines also a profile of the tail contribution of the surface tension. This correction results from the long range corrections to the normal and tangential elements of the pressure tensor. The fact that the first part $p^{(1)}(z_k)$ of the long range corrections to the pressure is equal for the normal and tangential elements, implies only one term for the long range correction to the surface tension defined in Eq. (22),

$$\gamma_{(\mathrm{lrc},4)}(z_k) = \frac{\pi}{2}\rho(z_k)\frac{V_s}{A}\int_{r_c}^{\infty} dr\int_{-r}^{r} d\Delta z \times \sum_{i=1}^{n_z}[\rho(z_i)-\rho(z_{i-1})]\frac{dU_{\mathrm{LJ},m}}{dr}[r^2-3(\Delta z)^2]. \tag{22}$$

As concerns the two last expressions, the total long range correction to the surface tension is obtained by summing up all the contributions to the local values of each bin and dividing the result by 2.

V. RESULTS AND DISCUSSION

In this work, we have performed several simulations as a function of the cutoff value and the system size. For each set of parameters listed in Table I, 5 simulations are carried out at temperatures varying from 299 K to 425 K. Only one temperature has been studied for the system using a cutoff of 22 Å because of the computational burden. The CPU times for each type of simulations are given in Table I. We see that the calculation of the long range corrections over 10 000 configurations takes about 10% of the MC simulation time. If the long range corrections were calculated at each cycle, the resulting CPU time would be of the same order of magnitude than the MC simulation time. These CPU times give an idea of the computational effort necessary for calculating the long range corrections.

Except for the total configurational energy, all the long range corrections to the pressure and to the surface tension have been computed once the simulations are completed. The second art of the long range correction to the energy, to the pressure components and to the surface tension have been calculated numerically using the Gaussian quadrature technique over 5 blocks of 2000 configurations. To do this, we have used the periodic boundary conditions along the z axis for the density profiles. Figure 1 displays the profiles along the axis for the two parts of the long range corrections to the total configurational energy for the largest value of L_z

This article is copyrighted as indicated in the article. Reuse of AIP content is subject to the terms at: http://scitation.aip.org/termsconditions. Downloaded to IP: 128.178.157.170 On: Mon, 15 Sep 2014 09:19:59

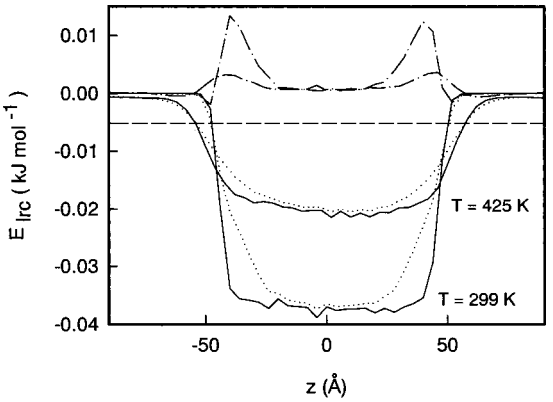

FIG. 1. The local long range corrections part to the configurational energy ($\mathrm{kJ\,mol^{-1}}$) along the *z*-axis for $T=299$ K and $T=425$ K with $r_c=13$ Å and $N=600$ molecules. $u_{\mathrm{lrc}}^{(1)}(z_k)$ (—); $u_{\mathrm{lrc}}^{(2)}(z_k)$ (–·–); $u_{\mathrm{lrc}}(z_k)=u_{\mathrm{lrc}}^{(1)}(z_k)+u_{\mathrm{lrc}}^{(2)}z_k)(\cdots)$. The dashed line represent a standard uniform correction to the total energy.

with a cutoff of 13 Å. We see that the u_{lrc} and $u_{\mathrm{lrc}}^{(1)}$ curves are very close to each other in the liquid phase, whereas they present some deviations in the interfacial regions. The deviations between the two curves in the interface regions decreases as the temperature increases. As expected, the second term $u_{\mathrm{lrc}}^{(2)}$ presents a positive peak in the interfacial region. This peak results from large density fluctuations in this zone. To evaluate the contribution of the second part of the total long range correction to the configurational energy, we have calculated the sum of the local corrections of each slab. The total long range energetic contributions in ($N=600$, $r_c=13$ Å) system is equal to $-0.74\ \mathrm{kJ\,mol^{-1}}$ at $T=299$ K, whereas the contributions of the first and second terms are $-0.84\ \mathrm{kJ\,mol^{-1}}$ and $0.10\ \mathrm{kJ\,mol^{-1}}$, respectively. At 299 K, the second term represents about 13% of the total contribution and only 9% at $T=425$ K. However, as it can be seen in Fig. 1, the neglect of the second part may effect slightly the interfacial properties. Therefore, neglecting the second term in our calculations amounts to overestimate the total long range correction of about 13% and represents nevertheless a rather reasonable approximation.

Figure 2 shows the density profiles at two temperatures

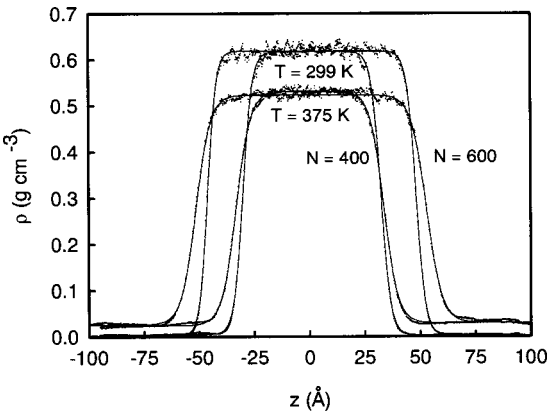

FIG. 2. Density profiles at two temperatures $T=299$ K and $T=375$ K for two systems ($N=400$ and $N=600$). Continuous lines represent the fitted tangent hyperbolic function. The temperature is indicated in each case.

TABLE II. Simulation results for *n*-pentane for different conditions of simulations. The coexisting densities and the thickness of the interface *d* are reported. The subscript indicates the accuracy of the last decimal(s). The number 0.456_{19} means 0.456 ± 0.019.

T/K	T_{conf}/K	$\rho_l/\mathrm{g\,cm^{-3}}$	$\rho_v/\mathrm{g\,cm^{-3}}$	d/Å
		$r_c=13$ Å, $N=400$		
299	298.8_5	0.615_6	0.004_2	8.0_4
350	350.3_4	0.560_{11}	0.009_4	10.6_7
375	374.2_4	0.529_{10}	0.018_4	13.7_{26}
400	399.6_8	0.491_{15}	0.040_{14}	15.3_{28}
425	425.6_{22}	0.456_{19}	0.077_{49}	21.7_{50}
		$r_c=15$ Å, $N=400$		
299	298.9_7	0.615_6	0.003_1	8.0_4
350	349.3_6	0.556_{12}	0.018_8	10.6_{14}
375	374.7_{20}	0.525_{13}	0.028_7	13.0_{18}
400	400.3_9	0.488_8	0.036_5	16.7_{16}
425	424.5_{10}	0.459_{20}	0.053_{11}	20.6_{34}
		$r_c=17$ Å, $N=400$		
299	298.8_8	0.617_6	0.003_1	8.4_8
350	350.4_{12}	0.566_{11}	0.012_3	11.3_{11}
375	375.4_{11}	0.531_8	0.025_4	12.7_{11}
400	400.0_{16}	0.485_{14}	0.032_4	15.6_{22}
425	425.3_{10}	0.454_{21}	0.049_8	20.1_{36}
		$r_c=13$ Å, $N=600$		
299	298.8_9	0.619_3	0.001_1	8.0_6
350	349.0_{10}	0.552_6	0.010_2	11.0_{16}
375	374.9_6	0.524_6	0.025_4	13.5_{20}
400	398.7_8	0.493_{11}	0.034_{10}	15.8_{20}
425	424.8_{15}	0.455_{10}	0.071_{20}	17.4_{28}
		$r_c=22$ Å, $N=600$		
299	299.0_6	0.619_6	0.002_1	8.4_7

for the two systems $N=400$ and $N=600$ molecules. The continuous lines represent the fit to the density profiles by a hyperbolic tangent function defined in Eq. (23),

$$\rho(z_k)=\frac{1}{2}(\rho_l+\rho_v)-\frac{1}{2}(\rho_l-\rho_v)\tanh\left(\frac{2(z-z_0)}{d}\right). \qquad (23)$$

In this equation, ρ_t and ρ_v are the coexisting densities of the liquid and vapor phases. The parameter z_0 indicates the location of the Gibbs surface and *d* is related to the interfacial thickness. Table II gives the liquid and vapor equilibrium densities with the estimation of the width of the interface for different values of r_c and two system sizes. Whatever the number of molecules and the cut of fradius we used, we check that the density profiles are symmetrical about the center of the box. These curves show two well established interfaces with a region of bulk liquid varying from 70 Å to 60 Å ($N=600$) and from 40 Å to 34 Å ($N=400$) as the temperature is increased from 299 K to 425 K. For a given number of molecules, we note also that the shape of the density profiles is not sensitive to the cutoff value. The simulated coexisting densities are shown in Fig. 3 with the corresponding experimental values. The resulting liquid and vapor densities are slightly dependent of the r_c value. Deviations of the liquid and vapor densities from experimental values decreased from 2.8% to 1.4% as the cutoff radius increases from 13 Å to 17 Å. Within the statistical uncertainty, we detect no change in the interfacial thickness when the cutoff is increased and

This article is copyrighted as indicated in the article. Reuse of AIP content is subject to the terms at: http://scitation.aip.org/termsconditions. Downloaded to IP: 128.178.157.170 On: Mon, 15 Sep 2014 09:19:59

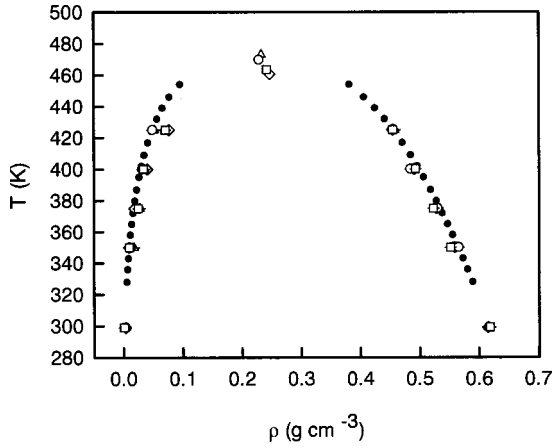

FIG. 3. Vapor–liquid coexistence density curve of *n*-pentane (●) experimental data; (◇) $N=400$, $r_c=13$ Å; (△) $N=400$, $r_c=15$ Å; (○) $N=400$, $r_c=17$ Å; (□) $N=600$, $r_c=13$ Å.

when we move from the system for 400 molecules to that with 600 molecules. We also observe that the interfacial thickness involves large error bars increasing with the temperature. The critical point[38] (T_c and ρ_c) is calculated by fitting the simulated coexistence density to the law of rectilinear diameters,

$$\frac{\rho_l+\rho_v}{2}=\rho_c+A(T-T_c) \tag{24}$$

and to the scaling law for the densities using an Ising-type critical exponent of $\beta=0.32$,

$$\rho_l-\rho_v=B(T-T_c)^{\beta}. \tag{25}$$

The critical temperatures and densities are listed in Table III. We check an excellent agreement between the computed and experimental values. The largest deviations result from the system with 400 molecules and a cutoff radius of 13 Å but are less than 2% for the critical temperature and 8% for the critical density. The prediction of the critical points is really improved as the cutoff is increased. As concerns the system with 400 molecules, the critical temperature estimated from our simulations is within 2% of the experimental value for $r_c=13$ Å and 0.7% for $r_c=15$ Å. For $r_c=17$ Å, the calculated critical temperature is in perfect agreement with the experimental value. The deviation between the critical density and the corresponding experimental value decreases from 8% to 0.4% when the cutoff radius is increased. At this point, it is interesting to note that the coexistence density and the critical points are better predicted with a larger cutoff. For a same cutoff radius, we observe a slight improvement in the prediction of the coexistence density and of the critical points with a larger box size in the direction normal to the interface.

TABLE III. Critical points of *n*-pentane. The experimental data are obtained through the correlations of Dortmund Data Bank (Ref. 39). The calculated critical temperatures and densities result from the fitting of the coexisting densities to Eq. (24) and Eq. (25). The critical pressure is calculated from Eq. (26).

	$r_c=13$ Å $N=400$	$r_c=15$ Å $N=400$	$r_c=17$ Å $N=400$	$r_c=13$ Å $N=600$	Expt.
T_c/K	460.6	473.0	469.9	463.4	469.7
ρ_c/g cm^{-3}	0.247	0.233	0.229	0.242	0.230
p_c/MPa	3.1	4.0	3.4	3.9	3.4

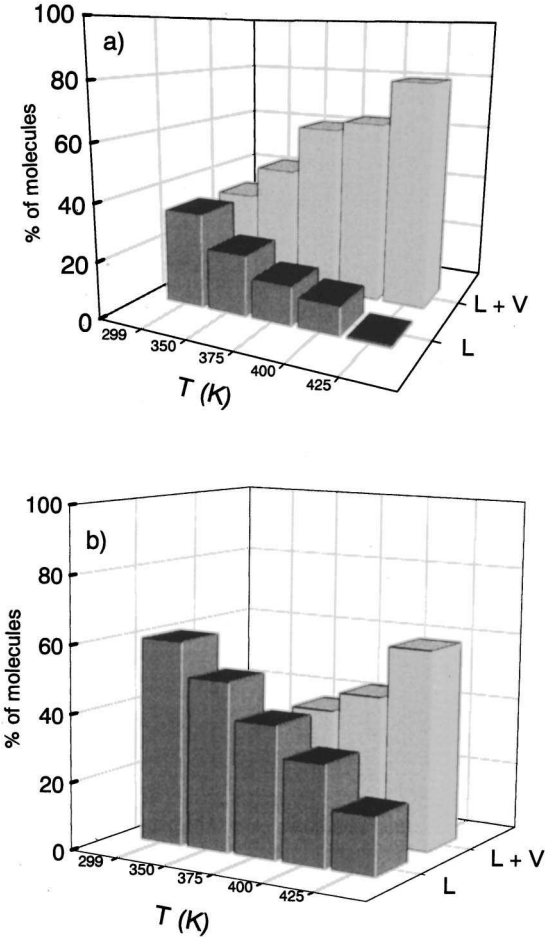

FIG. 4. % of C_5 molecules not leaving the liquid phase over 10 000 saved configurations (L) and % of molecules which were found at least once inside the liquid and vapor phases ($L+V$) for (a) $N=400$, $r_c=17$ Å and (b) $N=600$, $r_c=13$ Å, systems.

The efficiency of the algorithm using randomly two different displacements with equal probability can be tested by considering the displacements of pentane molecules along the direction perpendicular to the interface. We have calculated the percentage of molecules which have never left the liquid phase and the percentage of molecules which were found at least once inside the liquid and vapor phases over the 10 000 saved configurations. The results are represented in Fig. 4 for two different system sizes. As expected, the percentage of molecules which remained in the liquid phase decrease as the temperature increases, whereas the number of molecules which were at least once inside the liquid and vapor phases increases with the temperature. This last percentage gives an estimation of the number of transfers or exchange events between the vapor and liquid phases. These values can be different as a function of the number of molecules in the simulation cell but the variations of these percentages calculated in the two systems as a function of the temperature are quite similar. It is interesting to note that no

This article is copyrighted as indicated in the article. Reuse of AIP content is subject to the terms at: http://scitation.aip.org/termsconditions. Downloaded to IP: 128.178.157.170 On: Mon, 15 Sep 2014 09:19:59

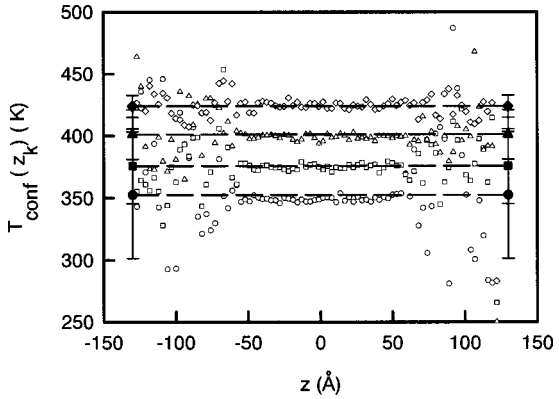

FIG. 5. Molecular configurational temperature profiles in the system with $N=600$ molecules. (○) $T=350$ K; (□) $T=375$ K; (△) $T=400$ K; (◇) $T=425$ K. We have added a line at the average molecular temperature calculated in the vapor region with its error bars representing the standard deviations.

pentane molecule has ever remained over the 10 000 sampled configurations in the vapor phase. All these results indicate a good sampling of our system in the z direction and confirms the efficiency of our algorithm for the translational moves.

The average configurational temperature calculated from Eq. (8) is reported in Table II and is in excellent agreement with the input temperature by yielding a maximum deviation of 0.2%. No particular trend is observed as a function of the cutoff value and of the number of molecules in the system. The equality of the temperatures in the vapor and liquid phases can be tested throughout the profiles of the configurational temperature along the z-axis. Figure 5 shows the $T_{\mathrm{conf}}(z_k)$ profiles for the temperatures $T=350$ K, 375 K, 400 K, and 425 K in the calculated system with 600 molecules. In addition, we have added a line corresponding to the average value calculated in the vapor region with the error bars. We see that these profiles can be considered as constant within the statistical fluctuations and show that the system is in thermal equilibrium as expected in a direct liquid–vapor simulation. To further investigate the profiles, we have calculated separately the mean temperature in the vapor and liquid phases by averaging over the corresponding slabs. As concerns the simulations at $T=299$ K, the very small number of molecules per slabs in the vapor phases causes a significant underestimation of the local temperature with larger oscillations. With $T=299$ K, it is not possible to extract a reliable average temperature from the profiles of the configurational temperature in the vapor phase, whereas the temperature is equal to 298.6 K in the liquid phase. The average temperature of the vapor phase is equal to $(352\pm51$ K) and $(424\pm9$ K) for the input temperature $T=350$ K and $T=425$ K, respectively. In the case of the average temperature in the liquid phase, we see that it is equal to $(349.0\pm1.6$ K) and $(424.9\pm2.4$ K) for the two Boltzmann temperatures $T=350$ K and $T=425$ K, respectively. The deviation between the average temperature in the vapor phase and the input temperature decreases from 1% to 0.2% as the temperature increases from 350 K to 425 K, whereas this deviation remains equal to 0.2% in the liquid phase. The decrease in the standard deviations of the average temperature in the vapor phases from 51 K to 9 K when the temperature varies from 350 K to 425 K underlines the improvement of the statistics with an increase of the number of molecules per slabs. It is worth noticing that the expression of the local configurational temperature yields temperatures in the liquid and vapor phases which match very well with the input temperature and can be therefore used to check the thermal equilibrium in a liquid–vapor interface system when the number of molecules in the vapor phase is sufficient.

As concerns the mechanical equilibrium, parts a and c of Fig. 6 show the profiles of the normal and tangential pressure tensor components calculated from Eq. (13) in which the long range corrections to the normal and tangential pressure are included, as a function of the temperature and for different systems. Within the error bars in the calculations, we see that the profiles of the local normal and tangential pressure tensors are constant in the liquid and vapor phases. At the interfaces, the tangential pressure exhibits two negative peaks suggesting that the surfaces are under tension whereas the normal pressure component is constant through the interface as imposed for a system at mechanical equilibrium with planar interfaces. The fact that $p_N(z_k)$ is constant and that $p_N(z_k)=p_T(z_k)$ away from interfaces does not depend on the size of the system and on the cutoff value. Figure 6(b) shows the corresponding $p_N(z_k)-p_T(z_k)$ profiles which are zero in the bulk phases and present two symmetric peaks in the interface region due to $p_T(z_k)$. The total surface tension can be measured as a function of z_k by integrating these profiles. Its value is constant in the bulk phases and increase at the interface. Figure 6(d) presents the difference between the configurational parts of the normal pressure component calculated by IK and MOP methods. To allow a direct comparison, we must recall that z_k corresponds the position of the volume element in the IK formalism and to the position of the plane in the MOP definition. We check that the difference by slab between the two profiles of the configurational parts of the pressure tensor are small compared to the value of the configurational part in the corresponding slab which can oscillate between 3 and 15 MPa as a function of the temperature and of the position in the box. In addition, we check that the average of the configurational part over the bins in the box is identical within 1% between the two definitions of the pressure tensor. Although the definitions of the configurational parts are different, we check the resulting profiles are very close confirming the validity of these both definitions for the liquid–vapor interface study. Figure 6(e) gives the profiles of the long range corrections parts to the normal and tangential pressure components $p^{(1)}_{N,\mathrm{lrc}}(z_k)$, $p^{(2)}_{N,\mathrm{lrc}}(z_k)$, and $p^{(2)}_{T,\mathrm{lrc}}(z_k)$, for the smaller and higher temperature in the system with $N=600$ molecules and a cutoff value of 13 Å. The shapes of these profiles resemble the profiles of the long range correction to the configurational energy. However, the second parts of the long range corrections to the normal and tangential pressure components may not be neglected and present two noticeable peaks in the interface region. The profiles of the second part of the long range corrections to the tangential and normal pressures are the same in the liquid and vapor regions and are different in the magnitude of the peaks in the interface. The difference between these two profiles gives the

This article is copyrighted as indicated in the article. Reuse of AIP content is subject to the terms at: http://scitation.aip.org/termsconditions. Downloaded to IP: 128.178.157.170 On: Mon, 15 Sep 2014 09:19:59

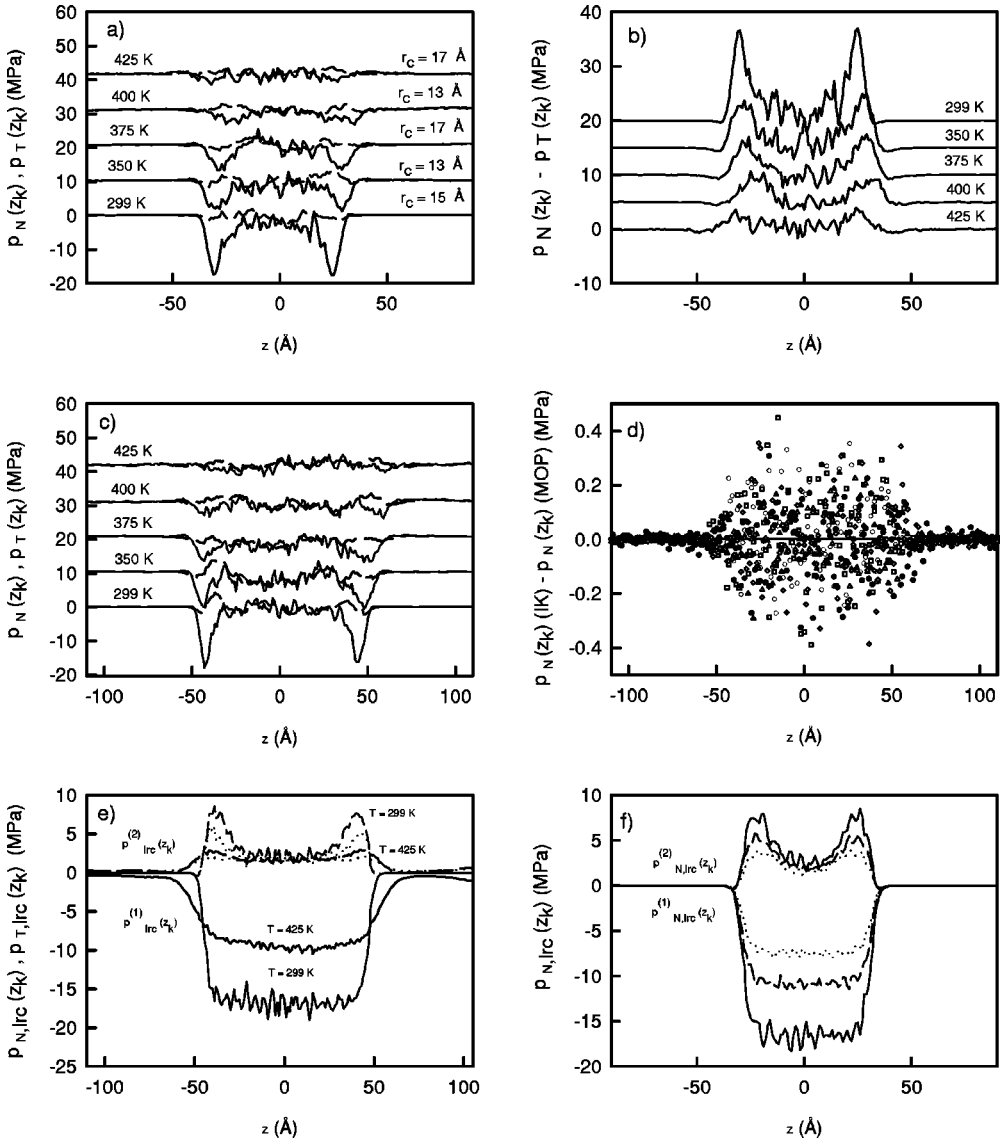

FIG. 6. (a) Tangential (—) and normal (– – –) pressure profiles and (b) the corresponding $p_N(z)-p_T(z)$ profiles with $N=400$ molecules at different cutoff values as a function of the temperature. (c) (—) $p_N(z)$ and (– – –) $p_T(z)$ pressure components calculated in the system with 600 molecules as a function of the temperature. The components of the pressure tensor with their differences are offset by 10 MPa for clarity. (d) Differences between the configurational parts of the pressure tensor calculated both IK and MOP definitions (○) $T=299$ K; (□) $T=350$ K; (△) $T=375$ K; (◇) $T=400$ K; (●) $T=425$ K. (e) Long range corrections parts $p^{(1)}_{N,\mathrm{lrc}}$ (—) and $p^{(2)}_{N,\mathrm{lrc}}$ (– – –) to the normal pressure component with the second part of the long range correction to the tangential pressure $p^{(2)}_{T,\mathrm{lrc}}$ (···) for two temperatures and for $N=600$ molecules. (f) Long range corrections parts to the normal pressure tensor profile calculated with $N=400$ molecules as a function the cutoff value (—) $r_c=13$ Å; (– – –) $r_c=15$ Å; (···) $r_c=17$ Å.

profile of the long range corrections to the surface tension. Figure 6(f) shows the long range corrections parts to the normal pressure tensor component in the system with 400 molecules as a function of the cutoff radius. This figure shows clearly that it is not possible to neglect the two parts of the long range corrections to the pressure components even with a cutoff radius of 17 Å.

In this paper, we demonstrate that it is possible to reach the mechanical equilibrium throughout the simulation cell under the condition that the two parts of the long range correction to the pressure components are applied. The vapor pressure is calculated by averaging the trace of pressure tensor in only the vapor phases to avoid larger statistical fluctuations in the liquid phase. These computed values are represented in Fig. 7 as a function of the temperature for different initial conditions. We observe that the calculated vapor pressure are in satisfactory agreement with the corresponding experimental values within important error bars. These vapor pressures are used to estimate the critical pressure throughout Eq. (26) of the Clausius–Clapeyron form,[9,41]

$$\ln p_v = A + \frac{B}{T}, \tag{26}$$

where A and B are constants. The critical pressure is calculated for each system and is reported in Table III. We see that the calculation of the critical pressure implies differences as a function of the system. Roughly, we notice that the experimental vapor pressure is bounded with our calculated pressure values with a maximum discrepancy of 0.6 MPa. This

This article is copyrighted as indicated in the article. Reuse of AIP content is subject to the terms at: http://scitation.aip.org/termsconditions. Downloaded to IP: 128.178.157.170 On: Mon, 15 Sep 2014 09:19:59

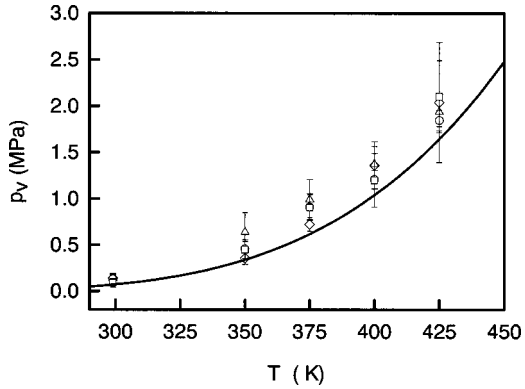

FIG. 7. The vapor pressures (MPa) of *n*-pentane as a function of the temperature. (◇) $N=400$, $r_c=13$ Å; (△) $N=400$, $r_c=15$ Å; (○) $N=400$, $r_c=17$ Å; (□) $N=600$, $r_c=13$ Å. The continuous curve represents the experimental values (Ref. 39).

deviation is of the same order of magnitude than the calculated error bar in the estimation of the critical pressure.[9] We check also that the critical pressure is accurately predicted in the system with $N=400$ molecules and a cutoff value of 17 Å. However, it is very difficult to extract from our simulations a reliable trend for the calculation of the critical pressure as function of the initial parameters (cutoff, system size). We only check that the critical pressure can be qualitatively predicted with the direct MC method.

TABLE IV. Computed surface tension (mN m^{-1}) γ_{IK} from the integration of the $p_N(z_k)-p_T(z_k)$ components profiles. The long range corrections to the surface tension (mN m^{-1}) are calculated from different expressions described in this paper. The total surface tension γ is computed from $\gamma_{IK}+\gamma_{(lrc,4)}$. The subscripts give the accuracy of the last decimal(s), i.e., 2.7_{18} is 2.7 ± 1.8.

T/K	γ_{IK}	$\gamma_{(lrc,1)}$	$\gamma_{(lrc,2)}$	$\gamma_{(lrc,3)}$	$\gamma_{(lrc,4)}$	γ
		$r_c=13$ Å, $N=400$				
299	13.2_{22}	5.4_1	4.6_2	4.5_1	4.7_1	17.9_{23}
350	8.0_{18}	4.4_2	3.4_2	3.4_1	3.6_1	11.6_{19}
375	5.2_{18}	4.0_1	2.6_2	2.7_1	2.9_1	8.1_{19}
400	3.0_{12}	3.4_2	1.9_2	2.1_1	2.3_1	5.3_{13}
425	2.2_{17}	3.0_2	1.1_3	1.5_1	1.6_1	3.8_{19}
		$r_c=15$ Å, $N=400$				
299	14.3_{12}	4.0_1	3.5_2	3.5_1	3.6_1	17.9_{13}
350	8.7_{19}	3.3_1	2.5_1	2.5_1	2.7_1	11.4_{20}
375	5.1_{28}	2.9_1	2.0_2	2.1_1	2.2_1	7.3_{30}
400	4.9_{13}	2.5_1	1.5_1	1.5_1	1.7_1	6.6_{14}
425	2.4_{17}	2.2_2	1.1_1	1.1_1	1.2_1	3.6_{18}
		$r_c=17$ Å, $N=400$				
299	14.3_{26}	3.2_1	2.8_1	2.7_1	2.8_1	17.1_{27}
350	8.2_{22}	2.7_2	2.1_1	2.1_1	2.2_1	10.4_{23}
375	5.2_{16}	2.3_1	1.7_2	1.7_1	1.8_1	7.0_{17}
400	3.3_{10}	1.9_2	1.2_2	1.3_1	1.4_1	4.7_{11}
425	2.7_{18}	1.7_2	0.9_1	0.9_1	1.0_1	3.7_{19}
		$r_c=13$ Å, $N=600$				
299	11.7_{25}	5.5_1	4.7_1	4.6_1	4.8_1	16.5_{26}
350	8.2_{29}	4.3_1	3.3_1	3.3_1	3.5_1	11.7_{30}
375	6.2_{18}	3.9_1	2.5_2	2.6_1	2.8_1	9.0_{19}
400	3.7_{20}	3.5_2	2.0_2	2.0_1	2.1_1	5.8_{21}
425	2.4_{16}	2.9_1	1.3_1	1.6_1	1.7_2	4.1_{18}
		$r_c=22$ Å, $N=600$				
299	14.6_{19}	1.9_1	1.5_1	1.7_1	1.7_1	16.3_{20}

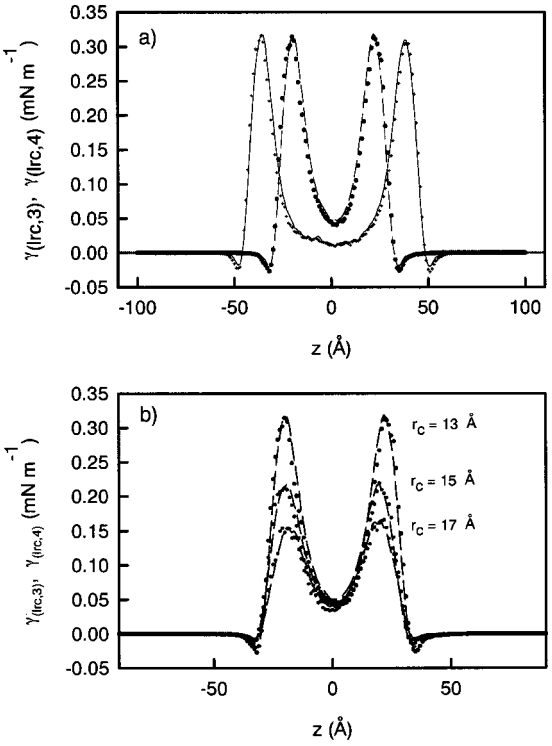

FIG. 8. (a) Long range corrections to the surface tension along the *z* axis for the *n*-pentane at 299 K using a cutoff at 13 Å. (+) $\gamma_{(lrc,3)}$, $N=600$; (—) $\gamma_{(lrc,4)}$, $N=600$; (●) $\gamma_{(lrc,3)}$ $N=400$; (—) $\gamma_{(lrc,4)}$ $N=400$. (b) Long range corrections to the surface tension calculated with $N=400$ molecules as a function of the cutoff value (●) $\gamma_{(lrc,3)}$; (– – –) $\gamma_{(lrc,4)}$.

We have calculated the surface tension using both Eq. (17) and Eq. (18) and we have checked that calculations using the Kirkwood–Buff formula and those resulted from the integration of the normal and tangential components of the pressure tensor match very well within the statistics of the simulations. This consistency between the two formalisms for the surface tension calculation validates the pressure tensor calculation from the IK definition. As a consequence, we have only reported in Table IV the values resulting from the integration of the $p_n(z_k)-p_T(z_k)$ profiles. In this table, long range corrections to the surface tension calculated using different expressions are listed as a function of the system. We check that the three expressions $\gamma_{(lrc,2)}$, $\gamma_{(lrc,3)}$, and $\gamma_{(lrc,4)}$ give similar results with a slightly larger value for $\gamma_{(lrc,4)}$. The tail corrections to the surface tension calculated by Eq. (19) are overestimated due to the fact that this very simplified expression neglects the density in the vapor phases and assumes that the interface has a zero thickness. The advantage of the $\gamma_{(lrc,3)}(z_k)$ and $\gamma_{(lrc,4)}(z_k)$ expressions is that they give tail corrections to the surface tension as a function of z and uses the current density profiles. Figure 8(a) gives the profiles of the long range corrections to the surface tension calculated by both expressions for two different systems. First, we see that the profiles are rigorously identical with two positive peaks at the interface towards the liquid region and two smaller negative peaks at the interface towards the vapor region. We see also that the local tail cor-

This article is copyrighted as indicated in the article. Reuse of AIP content is subject to the terms at: http://scitation.aip.org/termsconditions. Downloaded to IP: 128.178.157.170 On: Mon, 15 Sep 2014 09:19:59

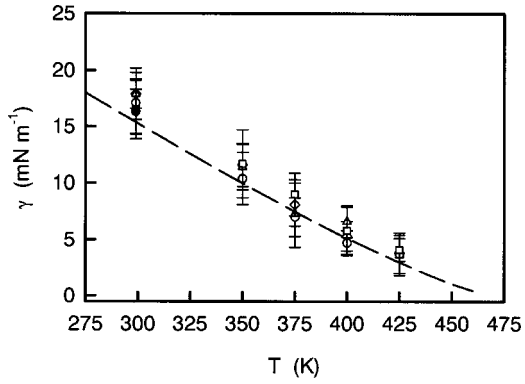

FIG. 9. Computed surface tension ($\mathrm{mN\,m^{-1}}$) as a function of the temperature for different systems (◇) $N=400$, $r_c=13$ Å; (△) $N=400$, $r_c=15$ Å; (○) $N=400$, $r_c=17$ Å; (□) $N=600$, $r_c=13$ Å; (●) $N=600$, $r_c=22$ Å. The dashed curve represents the data from Ref. 40.

rections to the surface tension are zero in the vapor phases. The profile calculated in the system with a larger L_z dimension differs from that calculated in a smaller box by a local value of the long range correction in the liquid phase closer to zero. This means that a larger value of L_z results in a more developed liquid bulk phase in the system with no interaction between the interfaces. Figure 8(b) shows the profiles of the long range corrections to the surface tension as a function of the cutoff value. These profiles present magnitudes of the positive peaks decreasing as the cutoff radius increases. No important change is detected for the local values of these long range corrections in the liquid phase as a function of the cutoff value. We have therefore checked that the system with $N=600$ molecules results in a more developed liquid phase and that the local values of the long range corrections to the surface tension in liquid phase is sensitive to the system size. However, we observe in Table IV that the total $\gamma_{(\mathrm{lrc},3)}$ and $\gamma_{(\mathrm{lrc},4)}$ values resulting from the sums over all the slabs are identical within the statistics although their profiles are different. The total surface tensions in which the long range corrections are calculated using Eq. (22) are represented in Fig. 9 as a function of the temperature and of the initial conditions. The deviations between the calculated surface tensions and those obtained from a generalized equation for surface tension from the triple point to the critical point[40] decrease from 13% to 9% when the cutoff radius is increased from 13 Å to 17 Å. This deviation is about the same for the two systems with $r_c=13$ Å. In addition, we observe that the total surface tension values are very little dependent of the cutoff radius if the long range corrections are applied. The agreement between the calculated surface tensions and those calculated from the generalized equation can be considered as very satisfactory considering the difficulty of estimating this value in molecular simulations.

VI. CONCLUSIONS

We have carried out MC calculations on the liquid–vapor interface of a flexible *n*-pentane molecule using various initial conditions. Our MC simulations take into account only the first part of the long range correction to the configurational energy within the Metropolis scheme and uses randomly two different displacements with equal probability. The efficient sampling of our system along the *z* axis has been revealed by an estimation of the number of transfers or exchange events between the vapor and liquid phases.

We have demonstrated that our direct MC simulations on a molecular system using a truncated and unshifted UA Lennard Jones potential for the nonbonded interactions reproduce the constancy of normal pressure along the axis perpendicular to the planar liquid–vapor interface on the conditions that the long range corrections parts to the normal pressure are applied. We have also checked that the normal and tangential pressure components are equal away from the interfaces. The mechanical equilibrium is satisfied for all the simulations in this work. We have used two different definitions for the calculation of the configurational part of the normal pressure component and we have shown that they lead to the same profiles.

The thermal equilibrium has been checked successfully from the calculation of the configurational temperature profiles. We observe that the temperature profiles are much noisier and oscillates around the Boltzmann temperature in the vapor phase, whereas they are constant and equal to the input temperature in the liquid phase. Except for the smaller temperature yielding poor statistics in the vapor phase, we have demonstrated that the average configurational temperature calculated in the vapor phase is identical to that of the liquid phase within the statistical fluctuations.

Once the thermodynamic equilibrium conditions have been checked, we have shown that the direct MC simulations predict critical densities and temperatures which become closer to the corresponding experimental value as the cutoff is increased. Using the larger cutoff (17 Å), the critical density is predicted within 0.4%, whereas the critical temperature is in perfect agreement with the experimental value. The prediction of the critical pressure is also excellent and this cutoff value. However, no clear trend can be drawn in the vapor pressures for different cutoff values. The calculation of the vapor pressure from the pressure tensor component is subject to larger statistical fluctuations but yields values quite in agreement with the corresponding experimental values.

We have also tested different analytical forms for the long range corrections to the surface tension. Except from a long range correction expression which overestimated the tail corrections because of unjustifiable approximations for our simulations, the three remaining expressions give the same results with the estimated error. The profiles of the long range corrections to the surface tension emphasizes that only the simulation box with the larger dimension along the *z* axis allow to obtain local values of the long range correction of the surface tension close to zero in the liquid phase in agreement with a fully developed liquid phase. However, the total long range correction to the surface tension is identical for our two system sizes. The dependence of the surface tension with system size and the cutoff radius is cancelled as the long range corrections are taken into account. We note also a very good agreement between the calculated surface tension and those resulted from a generalized equation within deviation of about 10%.

We plan to use the last version of the AUA potential[13]

This article is copyrighted as indicated in the article. Reuse of AIP content is subject to the terms at: http://scitation.aip.org/termsconditions. Downloaded to IP: 128.178.157.170 On: Mon, 15 Sep 2014 09:19:59

for the calculation of the vapor pressures and the surface tensions. Additional simulations using MD technique must be carried out to compare the equilibrium thermodynamic properties with those calculated from MC calculations. The MD technique can provide useful dynamical properties at the interface as for example the residence time of molecules at the interface.

ACKNOWLEDGMENTS

One of the authors (P.M.) wishes to acknowledge B. Rousseau, J. M. Simon, and P. Ungerer for interesting discussions about this work.

[1] A. Z. Panagiotopoulos, Mol. Phys. **67**, 813 (1987).
[2] A. Z. Panagiotopoulos, N. Quirke, M. Stapleton, and D. J. Tildesley, Mol. Phys. **63**, 527 (1988).
[3] A. Z. Panagiotopoulos, Mol. Simul. **9**, 1 (1992).
[4] B. Smit, S. Karaborni, and J. L. Siepmann, J. Chem. Phys. **102**, 2126 (1995).
[5] K. Esselink, L. D. J. C. Loyens, and B. Smit, Phys. Rev. E **51**, 1560 (1995).
[6] A. D. Mackie, B. Tavitian, A. Boutin, and A. H. Fuchs, Mol. Simul. **19**, 1 (1997).
[7] W. L. Jorgensen, J. D. Madura, and C. J. Swenson, J. Am. Chem. Soc. **106**, 6638 (1984).
[8] J. I. Siepmann, S. Karaborni, and B. Smit, Nature (London) **365**, 330 (1993).
[9] M. G. Martin and J. I. Siepmann, J. Phys. Chem. B **102**, 2569 (1998).
[10] S. Toxvaerd, J. Chem. Phys. **93**, 4290 (1990).
[11] P. Padilla and S. Toxvaerd, J. Chem. Phys. **94**, 5650 (1991).
[12] S. Toxvaerd, J. Chem. Phys. **107**, 12 (1997).
[13] P. Ungerer, C. Beauvais, J. Delhommelle, A. Boutin, B. Rousseau, and A. H. Fuchs, J. Chem. Phys. **112**, 5499 (2000).
[14] M. J. P. Nijmeijer, A. F. Bakker, C. Bruin, and J. H. Sikkenk, J. Chem. Phys. **89**, 3789 (1988).
[15] C. D. Holcomb, P. Clancy, and J. A. Zollweg, Fluid Phase Equilib. **75**, 185 (1992).
[16] C. D. Holcomb, P. Clancy, and J. A. Zollweg, Mol. Phys. **78**, 437 (1993).
[17] J. G. Harris, J. Phys. Chem. **96**, 5077 (1992).
[18] J. Alejandre, D. J. Tildesley, and G. A. Chapela, Mol. Phys. **85**, 651 (1995).
[19] G. A. Chapela, J. S. Rowlinson, and G. Saville, Faraday Discuss. Chem. Soc. **59**, 22 (1975).
[20] A. Trokhymchuk and J. Alejandre, J. Chem. Phys. **11**, 8510 (1999).
[21] M. Guo and B. C. Y. Lu, J. Chem. Phys. **106**, 3688 (1997).
[22] F. Goujon, P. Malfreyt, A. Boutin, and A. H. Fuchs, Mol. Simul. **27**, 99 (2001).
[23] B. D. Butler, G. Ayton, O. G. Jepps, and D. J. Evans, J. Chem. Phys. **109**, 6519 (1998).
[24] G. Ayton, O. G. Jepps, and D. J. Evans, Mol. Phys. **96**, 915 (1998).
[25] O. G. Jepps, G. Ayton, and D. J. Evans, Phys. Rev. E **62**, 4757 (2000).
[26] L. Lue and D. J. Evans, Phys. Rev. E **62**, 4764 (2000).
[27] J. H. Irving and J. G. Kirkwood, J. Chem. Phys. **18**, 817 (1950).
[28] A. Harasima, Adv. Chem. Phys. **1**, 203 (1958).
[29] J. P. R. B. Walton, D. J. Tildesley, and J. S. Rowlinson, Mol. Phys. **48**, 1357 (1983).
[30] J. P. R. B. Walton, D. J. Tildesley, and J. S. Rowlinson, Mol. Phys. **58**, 1013 (1986).
[31] B. D. Todd, P. J. Daivis, and D. J. Evans, Phys. Rev. E **51**, 4362 (1995).
[32] B. D. Todd, D. J. Evans, and P. J. Daivis, Phys. Rev. E **52**, 1627 (1995).
[33] J. G. Kirkwood and F. P. Buff, J. Chem. Phys. **17**, 338 (1949).
[34] E. Salomons and M. Mareschal, J. Phys.: Condens. Matter **3**, 3645 (1991).
[35] E. Salomons and M. Mareschal, J. Phys.: Condens. Matter **3**, 9215 (1991).
[36] M. Mecke, J. Winkelmann, and J. Fischer, J. Chem. Phys. **107**, 9264 (1997).
[37] M. Mecke, J. Winkelmann, and J. Fischer, J. Chem. Phys. **110**, 1188 (1999).
[38] J. S. Rowlinson and F. L. Swinton, *Liquid and Liquid Mixtures*, 3rd ed. (Butterworths, London, 1982).
[39] J. Gmehling, CODATA Bull. **58**, 56 (1985).
[40] G. R. Somayajulu, Int. J. Thermophys. **9**, 559 (1988).
[41] P. W. Atkins, *Physical Chemistry*, 4th ed. (Freeman and Company, New York, 1990), Chap. 6.

This article is copyrighted as indicated in the article. Reuse of AIP content is subject to the terms at: http://scitation.aip.org/termsconditions. Downloaded to IP: 128.178.157.170 On: Mon, 15 Sep 2014 09:19:59